JOURNAL OF SOLID STATE CHEMISTRY **133,** 77–81 (1997)
ARTICLE NO. SC977318

Synthesis and Characterization of New Quaternary Borocarbides RRh_2B_2C (R = Rare Earth)

Jinhua Ye,[1] Toetsu Shishido,* Takahiko Sasaki,* Toshitsugu Takahashi,* Kazuo Obara,* Ryunosuke Note,* Takehiko Matsumoto, and Tsuguo Fukuda*

*National Research Institute for Metals, 1-2-1 Sengen, Tsukuba, Ibaraki 305, Japan; and *Institute for Materials Research, Tohoku University, 2-1-1 Katahira, Aoba, Sendai 980, Japan*

Received January 16, 1997; accepted February 6, 1997

Arc-melting syntheses of RRh_2B_2C were carried out for all lanthanide elements except promethium. X ray diffraction revealed that new compounds exist for R = Y, La–Er (except Eu), and the stability of RRh_2B_2C decreases for the smaller lanthanide. The tetragonal a-axis of RRh_2B_2C was found to contract as R goes from La to Er. The c-axis, however, expands slightly. In accordance with the lattice parameter change, interatomic distances between Rh atoms decrease significantly from 2.7623 Å in $LaRh_2B_2C$ to 2.6552 Å in $ErRh_2B_2C$. The reduced stability of the RRh_2B_2C phase for the smaller rare earth is explained by the change in the crystallographic parameters with the size of R.

INTRODUCTION

Since the discovery of superconductivity with a T_c of 23 K in the Y–Pd–B–C system by Cava *et al.* (1), the interest in intermetallic compounds has been renewed, and a materials search for new quaternary borocarbides was performed extensively for a variety of rare earth (R) and transition metal (T) elements (2–6). The stability of RT_2B_2C compounds seems to strongly depend on the size of rare earth and transition metals. It is reported that RNi_2B_2C compounds could be obtained for lanthanides ranging from the large lanthanum down to the small lutetium atom (5). For larger transition metals Rh, Ir, Pd, and Pt, however, only larger lanthanides are reported to form the RT_2B_2C phase. No quaternary compound has been found for transition metals of Co and Fe.

The structure of the newly discovered quaternary borides RT_2B_2C is reported to be a derivative of the $ThCr_2Si_2$-type (7), which is very common for the well known magnetic ternary borides RT_2B_2 (T = Co, Fe) (8–9). Recently, we investigated the phase stability of the RT_2B_2 and RT_2B_2C compounds by focusing our concerns on the transition metal Rh. No RRh_2B_2 phases were found, and only the largest lanthanide La was reported to form the nonsuperconducting $LaRh_2B_2C$ (6). Arc-melting syntheses with starting composition of $R:Rh:B:C = 1:2:2:0$ and $1:2:2:1$ were carried out for several rare earth elements (10). It was found that no RRh_2B_2 compound was present, while RRh_2B_2C was obtained in multiphase form if carbon is added to the starting materials. The results suggested that the carbon atoms play an important role in the formation of the RT_2B_2C phase by adjusting the size of framework formed by the rare earth to enable various sizes of transition metals being accommodated in the $ThCr_2Si_2$ structure.

In the present work, to obtain a better understanding to the effects of rare earth and transition metals on the stability of quaternary borides, we carried out arc-melting synthesis with the starting composition of $R:Rh:B:C = 1:2:2:1$ for all lanthanides except promethium. The phase stability and crystal chemistry of the quaternary borocarbides will be discussed based on the results obtained for the new RRh_2B_2C compounds, as well as those reported for compounds consisting of other transition metals.

EXPERIMENTAL

RRh_2B_2C phases were prepared by arc-melting and annealing. The starting materials for arc-melting were lanthanide metals (99.9%), Rh powders (99.9%), crystallized boron (99.86%), and carbon powders (99.999%). These materials were mixed in an atomic ratio of $1:2:2:1$ and arc-melted under 1 atm argon atmosphere on a water-cooled copper hearth. The melted button was turned over and remelted three times to ensure homogeneity, followed by an annealing treatment in flowing Ar gas (200 ml min^{-1}) at 1473 K for 20 h (the sample was wrapped in tantalum foil).

X ray powder diffraction was carried out using the annealed samples on a rotating anode diffractometer

* To whom correspondence should be addressed.

0022-4596/97 $25.00

(JDX-3500) with monochromatized Cu$K\alpha$ radiation. Least-squares refinements of the lattice parameters, as well as Rietveld structural analysis, were performed to study the crystal chemistry of the compounds.

RESULTS AND DISCUSSION

X ray diffraction of the arc-melted alloys with starting composition of $R:Rh:B:C = 1:2:2:1$ (R = La–Lu, Y) revealed similarities in the main peak distribution of the diffraction patterns for lanthanides ranging from La to Er and Y. The observation indicates the existence of a similar phase in these arc-melted materials. The only exception is Eu, whose diffraction pattern was identified to be mostly EuB_6, and partly RhB and C. The difference in $Eu:Rh:B:C = 1:2:2:1$ arc-melted materials with others is due to serious evaporation of Eu during sample preparation. The melted button appears immiscible and unstable in air.

Rietveld structure analysis of the X ray diffraction pattern of the La-containing materials revealed a single phase product of $LaRh_2B_2C$, whose lattice parameters are very close to those reported for a single crystal by Siegrist *et al.* (6). In addition to the large La, new RRh_2B_2C compounds have formed for smaller lanthanides, besides the existence of some impurity phases. The diffraction patterns were carefully indexed and the lattice parameters of RRh_2B_2C phases were evaluated from least-squares refinements of the 2θ angles of more than 15 reflections ranging up to 100°. Crystallographic data of the new phases are listed in Table 1. The rare earth size (11) dependence of the a-, c-lattice parameters, as well as unit cell volume of the RRh_2B_2C compounds are plotted in Figs. 1a, 1b, and 1c. The radii for Ce^{3+}(1.034 Å) and Ce^{4+}(0.94 Å) are both indicated with a cross. For comparison with the data reported for RNi_2B_2C phases by Siegrist *et al.* (6), these are shown in the figure with small triangle marks.

TABLE 1
Crystallographic Data for RRh_2B_2C (Standard Deviations in Parentheses)

R	a (Å)	c (Å)	V (Å^3)	Rh–Rh (Å)
La	3.9065(6)	10.259(2)	156.56(4)	2.7623(2)
Ce	3.8594(9)	10.183(4)	151.68(6)	2.7290(3)
Pr	3.8744(5)	10.240(2)	153.71(3)	2.7396(2)
Nd	3.8508(4)	10.233(2)	151.74(3)	2.7229(1)
Sm	3.8239(5)	10.242(3)	149.76(4)	2.7039(2)
Gd	3.7882(9)	10.304(6)	147.87(8)	2.6786(3)
Tb	3.7777(4)	10.312(3)	147.17(4)	2.6712(1)
Dy	3.790(1)	10.252(4)	147.25(9)	2.6798(5)
Y	3.747(1)	10.401(5)	146.04(10)	2.6496(6)
Ho	3.7694(4)	10.284(2)	146.11(3)	2.6654(1)
Er	3.7550(7)	10.302(5)	145.26(7)	2.6552(3)

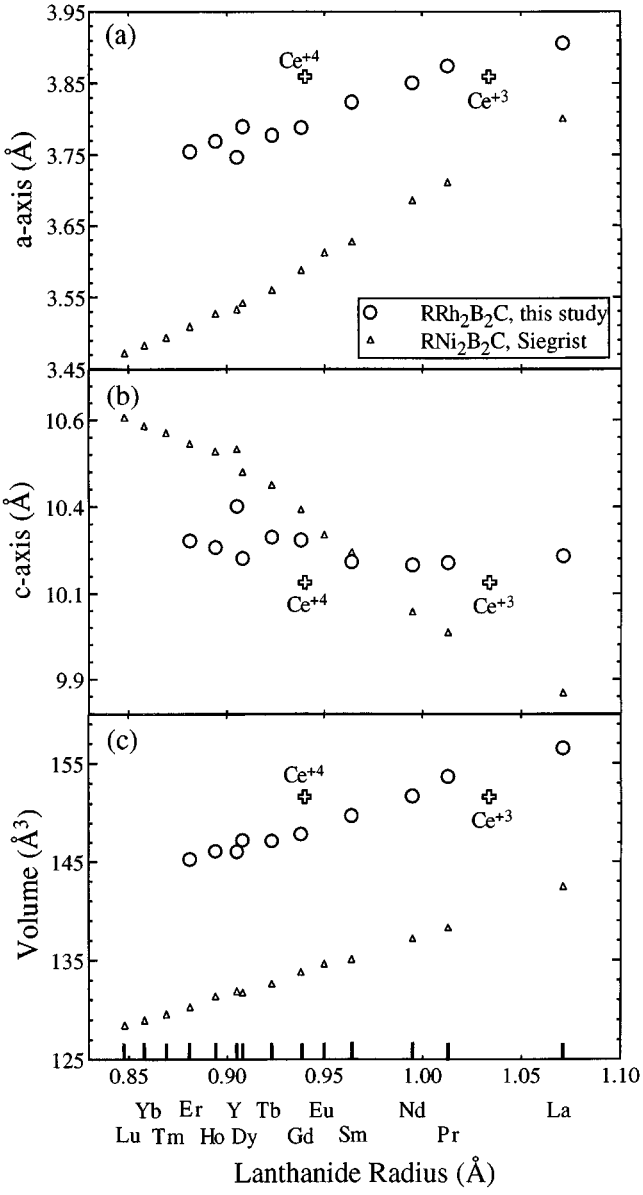

FIG. 1. Dependence of the (a) a-, (b) c-lattice parameters, and (c) unit cell volume of the RRh_2B_2C compounds on lanthanide size. The radii for Ce^{3+} and Ce^{4+} are indicated with a cross. Data reported for RNi_2B_2C by Siegrist *et al.* (6) are also shown in small triangles for a comparison.

Compared to RNi_2B_2C compounds, the data for RRh_2B_2C appear somewhat scattered. At present, we consider the scattering to come from the off-stoichiometry of carbon, which is known to affect the lattice parameters (10). Nevertheless, the tendency in variation of the crystallographic parameters of RRh_2B_2C with the size of the rare earth is obvious, except for cerium. Neither the trivalent nor the tetravalent radius of Ce follows the tendency, indicating an intermediate or mixed valence state of cerium between $+3$ and $+4$. The valence of Ce was estimated by interpolation to be approximately $+3.4$. Similar to the RNi_2B_2C

compounds, the tetragonal a-axis of $R\mathrm{Rh_2B_2C}$ also contracts with the size of the lanthanide atom, the c-axis, however, shows a slight expansion. This behavior is quite different from that observed for the $R\mathrm{Ni_2B_2C}$ compound, where the c-axis follows an opposite trend with the a-axis. In contrast to the scattering of the a- and c-axes, the overall volume (Fig. 1c), contracts almost linearly on the lanthanide size, in a manner similar to that observed in $R\mathrm{Ni_2B_2C}$. The contraction is small, from 156.56 Å^3 for $\mathrm{LaRh_2B_2C}$ to 145.26 Å^3 for $\mathrm{ErRh_2B_2C}$ (only 7.2%).

With decreasing size of the lanthanide atoms, reflection peaks of some impurity phases were observed, for instance, $\mathrm{CeB_2C_2}$ and $\mathrm{CeB_6}$ in Ce-containing arc-melted alloys. Except for these minor impurity phases, $R\mathrm{Rh_2B_2C}$ was obtained in the form of single phase for R ranging from La to Tb. For lanthanides smaller than Tb, an impurity phase with a strong diffraction peak at 2θ of about 38.75° was observed. This peak increases its intensity with further decrease in rare earth size.

For a clear view of this impurity phase, we plotted diffraction patterns of the Er-, Tm-, Yb-, and Lu-containing arc-melted materials in Figs. 2a, 2b, 2c, 2d, respectively, together with the diffraction pattern of $\mathrm{ErRh_3B_2}$ in Fig. 2e (powdered single crystals). It should be noted that due to the serious evaporation of Tm during arc-melting, no Tm-containing compound was obtained by the method. The diffraction pattern shown in Figs. 2b is for the sample prepared by high frequency heating in a carbon susceptor crucible, at 1873 K for 2 h. It can be seen that except for several peaks of $\mathrm{ErRh_2B_2C}$, indicated by circles in Fig. 2a and $\mathrm{YbB_2}$, marked with triangles in Fig. 2c, the remaining peaks in the diffraction patterns of Er-, Tm-, Yb-, and Lu-containing materials are very similar to those of $\mathrm{ErRh_3B_2}$. Thus the impurity phase in $R\mathrm{Rh_2B_2C}$ arc-melted alloys for smaller lanthanides is $R\mathrm{Rh_3B_2}$. The $R\mathrm{Rh_3B_2}$ phase increases with decreasing rare earth size. No $R\mathrm{Rh_2B_2C}$ peaks could be recognized for Tm and Yb, and only $\mathrm{LuRh_3B_2}$ was obtained for the smallest lanthanide Lu. Therefore, the size limitation for the formation of $R\mathrm{Rh_2B_2C}$ phases is determined to be Er.

Figure 3 shows the structure of the $R\mathrm{Rh_2B_2C}$ compounds. The structure can be viewed as a layered structure of RC NaCl-type layers with $\mathrm{Rh_2B_2}$ slabs. The $\mathrm{Rh_2B_2}$ layers contain a square-planar $\mathrm{Rh_2}$ array sandwiched between the boron planes. Each Rh atom is coordinated by four boron atoms to form a $\mathrm{RhB_4}$ tetrahedron, which share edges to form the extended $\mathrm{Rh_2B_2}$ slabs. The RC and $\mathrm{Rh_2B_2}$ layers connect to each other by the boron–carbon bonds.

While $R\mathrm{Ni_2B_2C}$ compounds were reported in phase-pure form for all the lanthanides from lanthanum to lutetium (6), for Rh, however, only La–Er and Y were observed to form the $R\mathrm{Rh_2B_2C}$ compounds, and an impurity phase of $R\mathrm{Rh_3B_2}$ increases its volume ratio to the quaternary borocarbides with decreasing lanthanide size. To obtain better understanding of the decreasing phase stability of the $R\mathrm{Rh_2B_2C}$ for the smaller lanthanide, interatomic distances between transition metals were calculated from the a-lattice

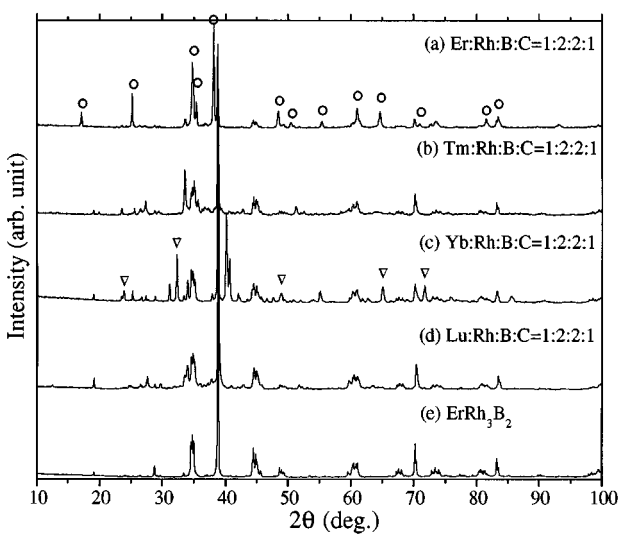

FIG. 2. X ray diffraction patterns showing impurity phases in $R:\mathrm{Rh}:\mathrm{B}:\mathrm{C} = 1:2:2:1$ arc-melted materials for smaller lanthanides (Tm, by high frequency power). Rare earth are Er in (a), Tm in (b), Yb in (c), and Lu in (d). Peaks indicated by circles belong to $\mathrm{ErRh_2B_2C}$, and by triangles to $\mathrm{YbB_2}$. For a comparison, the diffraction pattern of $\mathrm{ErRh_3B_2}$ is shown in (d).

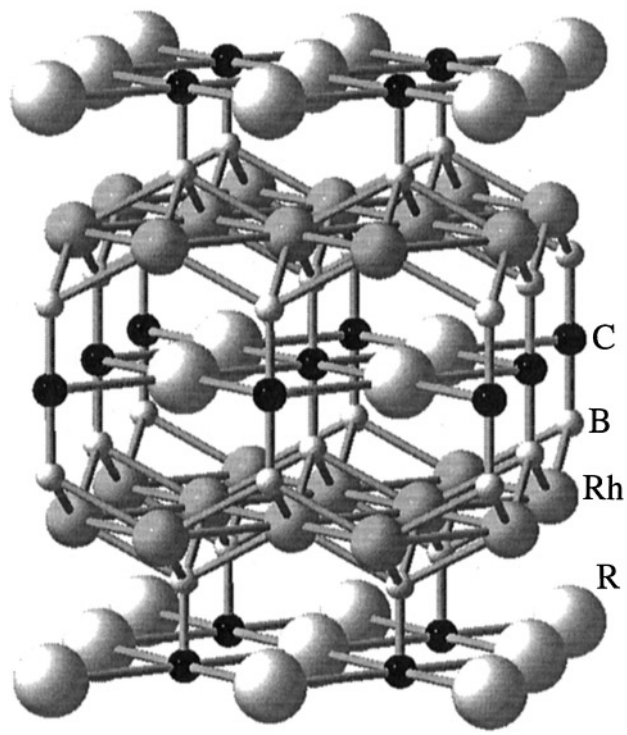

FIG. 3. Schematic diagram of the structure of $R\mathrm{Rh_2B_2C}$. The R, Rh, B, and C atoms are represented as large, medium, small bright, and small black spheres, respectively. Four unit cells are shown.

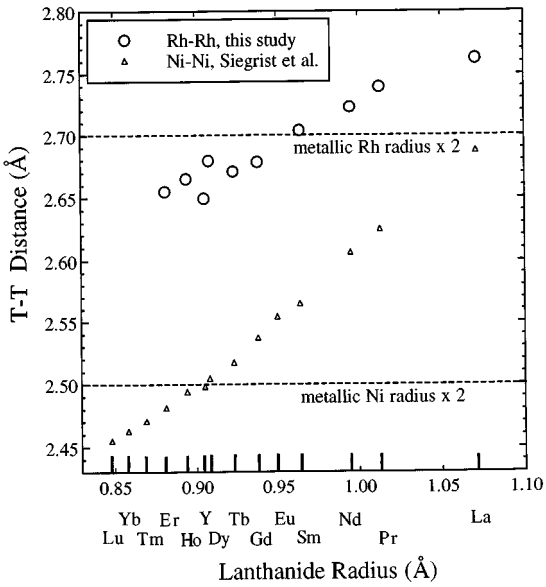

FIG. 4. Lanthanide size dependency of interatomic distances between transition metals in RT_2B_2C compounds. Circles represents those of Rh–Rh in RRh_2B_2C and triangles those of Ni–Ni in RNi_2B_2C compounds reported by Siegrist *et al.* (6).

parameter. The Rh–Rh distance is listed in Table 1 and shown in Fig. 4, along with the Ni–Ni distances for the RNi_2B_2C compounds as a comparison. In the figure, the two dotted lines represent the distances calculated from the radius of metallic rhodium and metallic nickel (12). It can be seen that the Rh–Rh distance decreases significantly from 2.7623 Å in $LaRh_2B_2C$ to 2.6786 Å in $GdRh_2B_2C$ and decreases further to 2.6552 Å in $ErRh_2B_2C$. The Rh–Rh distance in $GdRh_2B_2C$ and $ErRh_2B_2C$ are both shorter than the atomic distance expected from the metallic Rh diameter (2.70 Å), suggesting not only the strong metal–metal bonding in the structure, but also the decreasing stability of the RRh_2B_2C compounds. On the other hand, for the transition metal Ni, the Ni–Ni distances are 2.6877 Å in $LaNi_2B_2C$ and 2.5371 Å in $GdNi_2B_2C$. Both are longer than those calculated from metallic Ni diameter (2.50 Å). Even in the compound consisting of the smallest lanthanide Lu, the Ni–Ni distance is 2.4551 Å, about 1.8% shorter than the metallic nickel diameter. The contraction of T–T bond length in $LuNi_2B_2C$ is about the same as that in $ErRh_2B_2C$, which is the smallest lanthanide to form the RRh_2B_2C compounds. From these crystallographic data, it is easy to understand that the $ThCr_2Si_2$-type structure could readily accept all lanthanides for Ni, while for the transition metal rhodium, lanthanides smaller than Er are difficult to form the RRh_2B_2C phase.

RT_2B_2C compounds are conventionally strong coupling superconductors, in spite of their two-dimensional layered structure, which are in good analogy with the high T_c cuprates. Moreover, electronic band structure calculations of several Ni-based superconducting borocarbides (-nitrides) have revealed a common fact that there is a peak in the electronic density of states near the Fermi level, which is predominantly contributed from Ni 3*d* electrons (13–15). The calculations have led to a suggestion that the transition metals, as well as their bondings are important to superconductivity in borocarbides (6, 16). To examine relations between the structure parameters and superconductivity in RRh_2B_2C, we are now carrying out structure analyses of some of the RRh_2B_2C compounds grown in the form of single crystals (17) and a discussion on them will be made in a separate paper (18). Pressure effects on the structural and physical properties are also under investigation to reach better understandings on superconducting mechanism of the borocarbides.

CONCLUSION

Arc-melting syntheses of quaternary borocarbides were carried out for all lanthanide elements except promethium. In spite of the starting composition of $R:Rh:B:C = 1:2:2:1$ for each lanthanide, a nearly pure RRh_2B_2C phase was obtained only for the larger lanthanides La–Tb. The smaller lanthanides, Dy to Er, form a certain amount of RRh_3B_2 impurity phase besides the new RRh_2B_2C phase. The RRh_3B_2 phase increases its volume ratio to the RRh_2B_2C phase with the decreasing lanthanide size and becomes the only phase for the smallest lanthanide Lu.

The decreasing stability of the RRh_2B_2C phases for the smaller lanthanides can be explained from the variation of the crystallographic parameters of the phases. In accordance with the decreasing lanthanide size, the atomic distance between transition metal atoms (Rh) decreases significantly, and becomes 1.7% shorter than the distance expected from the radius of metallic rhodium in $ErRh_2B_2C$. The result is consistent with the observation that RRh_2B_2C compounds are difficult to form for lanthanides smaller than Er.

ACKNOWLEDGMENT

This work was performed under the interuniversity cooperative research program of Institute for Materials Research, Tohoku University.

REFERENCES

1. R. J. Cava, H. Takagi, B. Batlogg, H. W. Zandbergen, J. J. Krajewski, W. F. Peck, Jr., R. B. Dover, R. J. Felder, T. Siegrist, K. Mizuhashi, J. O. Lee, H. Eisaki, S. A. Carter, and S. Uchida, *Nature* **367,** 146 (1994).
2. R. J. Cava, H. Takagi, H. W. Zandbergen, J. J. Krajewski, W. F. Peck, Jr., T. Siegrist, B. Batlogg, R. B. van Dover, R. J. Felder, K. Mizuhashi, J. O. Lee, H. Eisaki, and S. Ushida, *Nature* **367,** 252 (1994).
3. R. J. Cava, B. Batlogg, T. Siegrist, J. J. Krajewski, W. F. Peck, Jr., S. Carter, R. J. Felder, H. Takagi, and R. B. van Dover, *Phys. Rev. B* **49,** 12384 (1994).

4. L. C. Gupta, R. Nagarajan, Z. Hossain, C Mazumdar, S. K. Dhar, C. Godart, C. Levy-Clement, B. D. Padalia, and R. Vijayaraghavan, *J. Magn. Magn. Mat.* **140–144,** 2053 (1995).
5. T. Siegrist, H. W. Zandbergen, R. J. Cava, J. J. Krajewski, and W. F. Peck, Jr., *Nature* **367,** 254 (1994).
6. T. Siegrist, R. J. Cava, J. J. Krajewski, and W. F. Peck, Jr., J. *Alloys Compounds* **216,** 135 (1994).
7. Z. Ban and M. Sikirica, *Acta Crystallogr.* **18,** 594 (1965).
8. B. Rupp, P. Rogl, and F. Hulliger, *J. Less-Common Metals.* **135,** 113 (1987).
9. K. Niihara, T. Shishido, S. Yajima, *Bull. Chem. Soc. Jpn.* **46,** 1137 (1973).
10. J. Ye, T. Shishido, T. Sasaki, T. Matsumoto, and T. Fukuda [submitted to *J. Alloys Compounds*].
11. A. Iandelli and A. Palenzona, *in* "Handbook on the Physics and Chemistry of Rare Earths" (K. A. Gschneider and L. Eyring, Ed.), Chap. 13, Vol. 2. North-Holland, Amsterdam, 1984.
12. W. B. Pearson, *in* "The Crystal Chemistry and Physics of Metals and Alloys." Wiley, New York, 1972.
13. L. F. Marttheiss, *Phys. Rev. B* **49,** 13279 (1994).
14. L. F. Marttheiss, T. Siegrist, and R. J. Cava, *Solid State Commun.* **91,** 587 (1994).
15. D. J. Singh and W. E. Pickett, *Phys. Rev. B* **51,** 8668 (1995).
16. C. C. Lai, M. S. Lin, Y. B. You, and H. C. Ku, *Phys. Rev. B* **51,** 420 (1995).
17. J. Ye, T. Shishido, T. Kimura, T. Matsumoto, and T. Fukuda, *Acta Crystallogr. C* **52,** 2652 (1996).
18. J. Ye, T. Shishido, T. Kimura, T. Matsumoto, and T. Fukuda [in preparation].